

Frequency-encoded linear cluster states with coherent Raman photons

Dale Scerri,* Ralph N. E. Malein, Brian D. Gerardot, and Erik M. Gauger†
SUPA, Institute of Photonics and Quantum Sciences,
Heriot-Watt University, EH14 4AS, United Kingdom.
 (Dated: September 5, 2022)

Entangled multi-qubit states are an essential resource for quantum information and computation. Solid-state emitters can mediate interactions between subsequently emitted photons via their spin, thus offering a route towards generating entangled multi-photon states. However, existing schemes typically rely on the incoherent emission of single photons and suffer from severe practical limitations, for self-assembled quantum dots most notably the limited spin coherence time due to Overhauser magnetic field fluctuations. We here propose an alternative approach of employing spin-flip Raman scattering events of self-assembled quantum dots in Voigt geometry. We argue that weakly driven hole spins constitute a promising platform for the practical generation of frequency-entangled photonic cluster states.

Introduction – Robust highly-entangled ‘cluster’ states are of paramount importance for measurement-based (‘one-way’) quantum computation^{1–4}. The experimental challenges of obtaining high-dimensional cluster states can be significantly reduced by probabilistically ‘fusing’ qubits from adjacent 1D linear cluster (LC) states^{5–7}, or ‘glueing’ together micro-clusters⁸. Several platforms for generating photonic LC states have been proposed, varying from condensed matter emitters such as quantum dots^{6,9–13} and crystal defects^{11,14} to parametric downconversion^{15,16}, all presenting their own sets of advantages and challenges. Solid-state-based protocols typically make use of pulsed excitations to drive optical transitions in a matter qubit to entangle the emitter’s spin degree of freedom with the polarisation of subsequently emitted photons. Encouragingly, a photonic LC of length two (LC₂) has recently been demonstrated experimentally, showing that the entanglement in this setup could persist for up to five consecutively emitted photons¹³.

Whilst conceptually elegant and ostensibly deterministic, real-world imperfections pose significant barriers to the experimental realisation of protocols such as the ones introduced by Refs. 9, 10, 17, and 18. These include phonon-dephasing of excited states¹⁹, modified selection rules as a consequence of hole mixing as well as a transverse (Voigt) component of the Overhauser field^{20–23}, and limited spin lifetimes due to Overhauser field fluctuations^{20,24–27}. Decoupling techniques^{28–34} and control of the nuclear environment^{27,35–37} overcome the latter but provide no remedy for other error sources. Unavoidable shortcomings of real quantum dots thus severely limit the size of cluster state achievable and render genuinely deterministic operation impractical for the current experimental state-of-the-art.

In contrast to direct pulsed excitation, we here propose employing a weak continuous wave (c.w.) laser to drive the Zeeman-detuned transitions of a hole-spin for entangling the spin with the frequency of Raman scattered photon. We show such a setup overcomes the experimental barriers suffered by previous schemes: in particular, our protocol is impervious to phonon dephasing, robust against fluctuations of the Overhauser field, and unaf-

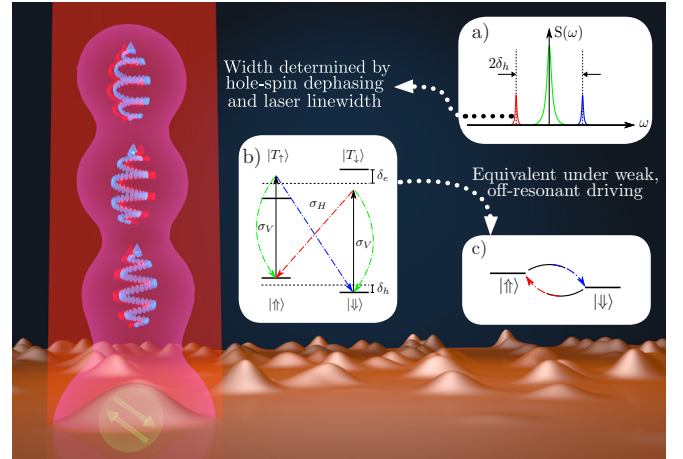


FIG. 1: **Background:** artistic depiction of our protocol. **Inset a):** Schematic of the emission spectrum showing the presence of the Raman sidebands. **Inset b):** Schematic illustration of the scattering processes involving the two ground hole-spin states. The black arrows denote the laser driving on resonance with the unperturbed transitions (dashed lines), whereas the green, red and blue arrows denote the Rayleigh, red detuned and blue detuned events, respectively. **Inset c):** Simple schematic of the scattering processes involved in the weak, detuned driving limit.

ected by heavy-hole (hh) light-hole (lh) mixing. This comes at the cost making the protocol probabilistic, however, we show that LC states of sufficient length to serve as building blocks for fusion⁵ can be produced at high rates and with high fidelity based on current experimental capabilities. Further, extended versions of our protocol mitigating its probabilistic limitations (whilst keeping its robustness) are possible. Our work thus shows that the significant divide between elegant theoretical proposals and experimental progress in the generation of linear cluster states can be overcome.

Model – Despite its many attractive features for quantum metrology and quantum information^{24,38}, the spin

of an electron trapped in an epitaxial quantum dot suffers from rapid ensemble dephasing due to the hyperfine interaction with $\sim 10^4 - 10^6$ randomly fluctuating nuclear spins of the host material. This typically results in a loss of coherence on the order of nanoseconds^{23–26}. By contrast, the p -orbital-like wavefunction of hole spin states vanishes at the location of the nuclear spins, which suppresses the Fermi-contact interaction, leaving only the much weaker dipole-dipole interaction as the main source of dephasing^{21,39–41}. Strain lifts the degeneracy of the $J = 3/2$ hole states, resulting in energetically split heavy ($J_z = \pm 3/2$) and light ($J_z = \pm 1/2$) holes; the former being closer to the valence band edge (see Fig. 1). However, chiefly due to strain anisotropy in the QD, a finite admixture of these states is always present (the effects on hole-based multi-photon entanglement schemes are briefly discussed in Appendix Sec F 3). In the following, we denote the (Zeeman) spin state of the heavy hole as $|\uparrow\rangle$ and $|\downarrow\rangle$ whereas the electron spin states are $|\uparrow\rangle$ and $|\downarrow\rangle$. In this notation, the positively charged X^{1+} transition $|\uparrow\rangle \leftrightarrow |T_\uparrow\rangle = |\uparrow\downarrow, \uparrow\rangle$ couples to σ^- polarised light and $|\downarrow\rangle \leftrightarrow |T_\downarrow\rangle = |\uparrow\downarrow, \downarrow\rangle$ to σ^+ polarised light. In the absence of an external magnetic field, both $|\downarrow\rangle \leftrightarrow |T_\uparrow\rangle$ and $|\uparrow\rangle \leftrightarrow |T_\downarrow\rangle$ transitions are dipole-forbidden. However, an external magnetic field in Voigt geometry unlocks those diagonal Raman transitions (see Fig. 1)⁴². For weakly off-resonantly driven hole spins, the width of these Raman transitions is solely limited by the laser linewidth and ground state spin dephasing^{43,44}, making them attractive candidates for single photon sources, as well as being attractive spin-spin qubit entanglers due to the spin's rich level scheme and selection rules^{45,46}.

Wishing to exploit such Raman photons for LC generation we consider a self-assembled quantum dot in the Voigt geometry, with the applied magnetic field B strong enough to dominate over nuclear Overhauser field fluctuations (see Appendix Sec B). The applied B -field (w.l.o.g. along the x -axis) then defines the basis of spin eigenstates. We also include a c.w. laser field that is resonant with the unperturbed transition of the QD (Fig. 1a). In a frame rotating with the laser frequency (after performing the RWA), the Hamiltonian in the Zeeman basis reads

$$\begin{aligned}
H = & \delta_h (|\uparrow\rangle \langle\uparrow| - |\downarrow\rangle \langle\downarrow|) + \delta_e (|T_\downarrow\rangle \langle T_\downarrow| - |T_\uparrow\rangle \langle T_\uparrow|) \\
& - \left(\frac{\Omega_H}{2} |T_\uparrow\rangle \langle\downarrow| + \frac{\Omega_H}{2} |T_\downarrow\rangle \langle\uparrow| + \frac{\Omega_V}{2} |T_\downarrow\rangle \langle\downarrow| \right. \\
& \left. + \frac{\Omega_V}{2} |T_\uparrow\rangle \langle\uparrow| + \text{H.c.} \right), \quad (1)
\end{aligned}$$

where $\delta_{e,h}$ are the electron and hole Zeeman splittings, respectively, $\Omega_{H/V}$ are the Rabi frequencies for the horizontally/vertically-polarised transitions, and H.c. denotes the Hermitian conjugate.

Protocol – Fig. 1b shows that the emission of blue and red-detuned Raman spin-flip photons from a single quantum dot must alternate, provided that the scattering rate is faster than the hole spin-flip time. We build

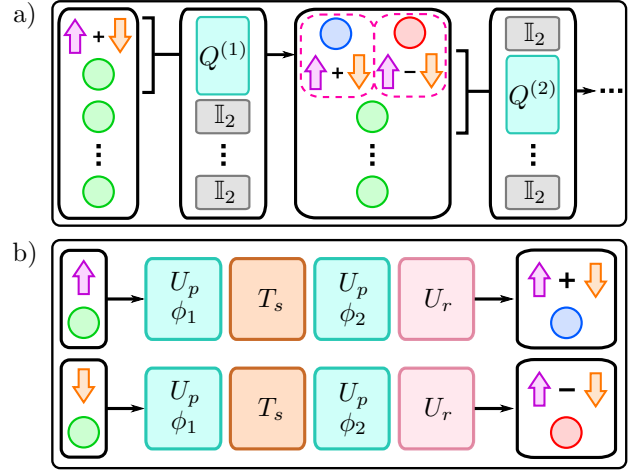


FIG. 2: **a)**: Diagrammatic representation of the spin-photon entangling process for the first emitted photon. The initial spin state ($|\uparrow\rangle + |\downarrow\rangle$) and first laser photon to be scattered (upmost green circle) undergo a joint transformation $Q^{(1)}$, resulting either in a red or a blue-detuned Raman photon that is entangled with the hole spin. $Q^{(2)}$ includes the second Raman process and entangles the newly scattered with the previous photon. **b)**: Break-down of the $Q^{(i)}$ operation through its action on spin basis states: the sequence of operations transforms includes two periods of free spin precession U_p , the Raman scattering process T_S , and a $\pi/2$ Y -rotation U_r . A full matrix representation of $Q^{(i)}$ is given in the Appendix Sec. C.

on this correlation between spin and photon colour to develop a protocol for generating an entangled LC state. As an intrinsic drawback of Raman spin-flips, the time at which a photon is scattered is not known prior to its detection. In the following, we assume that there is exactly one Raman scattering event per time-bin T_B (albeit at a random time within the bin, see Fig. S5.). The overall probability and ways of circumventing this limitation⁴⁷ will be discussed later. Fig. 2 contains a diagrammatic representation of a successful run of our protocol. Let us trace the evolution of the joint spin-photon-state step by step: we start with the hole spin initialised in the superposition state $|\uparrow\rangle + |\downarrow\rangle$ (ignoring normalisation factors) and precessing at its Larmor frequency. Let the accumulated phase prior to the first scattering event be $\phi_1 = \delta_h \tau_1$, then a Raman spin flip evolves the state to

$$e^{-i\frac{\phi_1}{2}} |\uparrow\rangle + e^{i\frac{\phi_1}{2}} |\downarrow\rangle \rightarrow e^{-i\frac{\phi_1}{2}} |\downarrow B_1\rangle + e^{i\frac{\phi_1}{2}} |\uparrow R_1\rangle, \quad (2)$$

where the labels $B_1(R_1)$ inside the ket denote the first emitted blue (red) photon. A subsequent period of free precession $\tau_2 = T_B - \tau_1$ until the end of the time-bin T_B results in a phase $\phi_2 = \delta_h \tau_2$. We now apply a $\pi/2$

Y-rotation ($Y_{\frac{\pi}{2}}$), yielding the state

$$\begin{aligned} & e^{-i\frac{\chi_1}{2}} |\uparrow B_1\rangle + e^{-i\frac{\chi_1}{2}} |\downarrow B_1\rangle \\ & + e^{i\frac{\chi_1}{2}} |\uparrow R_1\rangle - e^{i\frac{\chi_1}{2}} |\downarrow R_1\rangle, \end{aligned} \quad (3)$$

where $\chi_1 := \phi_1 - \phi_2$. The next Raman scattering event will have been preceded by another spin precession angle ϕ_3 resulting in

$$\begin{aligned} & e^{-i\frac{\phi_3}{2}} e^{-i\frac{\chi_1}{2}} |\downarrow B_1 B_2\rangle + e^{i\frac{\phi_3}{2}} e^{-i\frac{\chi_1}{2}} |\uparrow B_1 R_2\rangle \\ & + e^{-i\frac{\phi_3}{2}} e^{i\frac{\chi_1}{2}} |\downarrow R_1 B_2\rangle - e^{i\frac{\phi_3}{2}} e^{i\frac{\chi_1}{2}} |\uparrow R_1 R_2\rangle. \end{aligned} \quad (4)$$

The spin precesses further by ϕ_4 before we apply the next $Y_{\frac{\pi}{2}}$ rotation, yielding

$$\begin{aligned} & e^{-i\frac{\phi_3}{2}} e^{i\frac{\phi_4}{2}} e^{-i\frac{\chi_1}{2}} |\downarrow B_1 B_2\rangle + e^{i\frac{\phi_3}{2}} e^{-i\frac{\phi_4}{2}} e^{-i\frac{\chi_1}{2}} |\uparrow B_1 R_2\rangle \\ & + e^{-i\frac{\phi_3}{2}} e^{i\frac{\phi_4}{2}} e^{i\frac{\chi_1}{2}} |\downarrow R_1 B_2\rangle - e^{i\frac{\phi_3}{2}} e^{-i\frac{\phi_4}{2}} e^{i\frac{\chi_1}{2}} |\uparrow R_1 R_2\rangle \\ & := e^{-i\frac{\chi_2}{2}} e^{-i\frac{\chi_1}{2}} |\downarrow B_1 B_2\rangle + e^{i\frac{\chi_2}{2}} e^{-i\frac{\chi_1}{2}} |\uparrow B_1 R_2\rangle \\ & + e^{-i\frac{\chi_2}{2}} e^{i\frac{\chi_1}{2}} |\downarrow R_1 B_2\rangle - e^{i\frac{\chi_2}{2}} e^{i\frac{\chi_1}{2}} |\uparrow R_1 R_2\rangle. \end{aligned} \quad (5)$$

Let us stop at this point and, for clarity, consider the resulting state without its free precession phases

$$|\downarrow B_1 B_2\rangle + |\uparrow B_1 R_2\rangle + |\downarrow R_1 B_2\rangle - |\uparrow R_1 R_2\rangle. \quad (6)$$

Using the photon qubit encoding $|B_i\rangle = |1_i\rangle$, $|R_i\rangle = |0_i\rangle$, the state following the final $Y_{\frac{\pi}{2}}$ rotation it is given by

$$\begin{aligned} & |\uparrow 1_1 1_2\rangle + |\downarrow 1_1 1_2\rangle + |\uparrow 1_1 0_2\rangle - |\downarrow 1_1 0_2\rangle \\ & + |\uparrow 0_1 1_2\rangle + |\downarrow 0_1 1_2\rangle - |\uparrow 0_1 0_2\rangle + |\downarrow 0_1 0_2\rangle. \end{aligned} \quad (7)$$

In Appendix Sec D, we show that, whether the spin is measured to be in the $|\uparrow\rangle$ or $|\downarrow\rangle$ state, the resulting photonic state ($S_+^{(2)}$ or $S_-^{(2)}$, respectively) indeed corresponds to LC_2 . Further, we show that the above protocol generalises trivially to the production of LC states of arbitrary length. Crucially, reintroducing the above precession phases keeps the state local-unitarily (LU) equivalent to LC_2 . The phases become known post-measurement through the timestamps of the detection clicks, and in the Appendix, we discuss how to make allowances for them for a tomographic reconstruction of the LC state.

Results – We now analyse the quality and success probability of our protocol. We begin with the rate for Raman scattering events followed by the success probability of a string of n Raman photons with one per time-bin. Fig. 3a shows the Raman scattering rate and its dependence on both B and the (vertically-polarised) driving Ω_V . Comparison with numerical simulations shows that this rate is well-approximated by the transition probability obtained by treating the weak driving field perturbatively to sec-

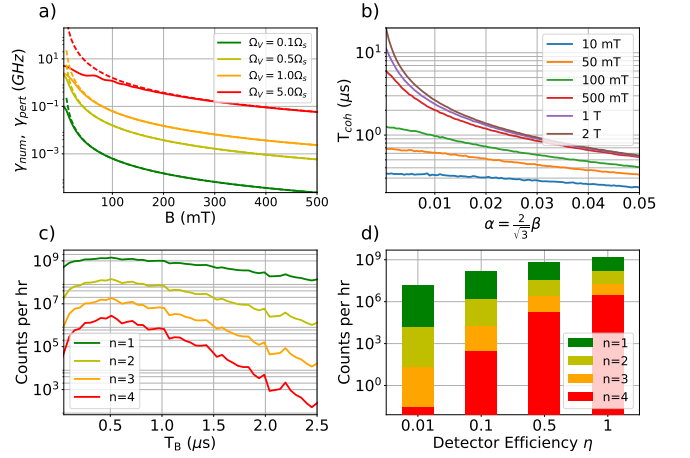


FIG. 3: **a)**: Perturbative calculation γ_{pert} (dashed) and numerical value γ_{num} (solid) of the Raman scattering rate as a function of B for various driving strengths. **b)**: Coherence time for the pseudospin initially prepared perpendicular to the applied external magnetic field with mixing factor $\alpha = \frac{2}{\sqrt{3}}\beta$ for various external field strengths. The Overhauser field was taken to have a spread of 14mT. **c)**: Number of successful n -photon correlations per hour against T_B , with $\eta = 1$ for the ideal scenario $B = 100\text{mT}$, $\Omega = 0.2\gamma/\sqrt{2}$, and $g_h^x = 0.1$. **d)**: Success probabilities optimised for $T_B = 500\text{ ns}$ [by minimising Eqn. (9)] against η .

ond order (see Appendix Sec A)

$$\gamma_{pert} = \frac{1}{8} \frac{\Omega_V^2 \gamma}{\Delta^2}, \quad (8)$$

provided $B \gtrsim 100\text{ mT}$ and $\Omega_V \lesssim \Omega_{sat}$. We proceed to determine the optimal duration T_B (i.e. the free precession time between Y -rotations) for maximising the probability of obtaining a single Raman event per time bin. Adopting $B = 100\text{ mT}$ and $\Omega_V = 0.2\gamma/\sqrt{2}$ (taking $\gamma = 1\text{ ns}^{-1}$ as the spontaneous emission rate), we calculate the number of successful trials with one Raman photon per T_B interval in n successive time-bins. Fig. 3c illustrates the results of Monte-Carlo simulations for $n = 1$ to 4 scattering events, suggesting that $T_B \approx 0.5\ \mu s$ is close to optimal. We have the relation $P_s(n) = P_s(1)^n$ between the success probability for a single bin and that of n bins.

Apart from addressing the possibility of having no Raman events within a time-bin, we also need to account for the possibility of ‘false-positives’, i.e. detecting only one of multiple Raman events occurring in a single time-bin, due to a photon detection efficiency $\eta < 1$ ⁴⁸. The probability of such n photon false positives, $P_{fp}(n)$, is given by the simple relation:

$$\begin{aligned} P_{fp}(n) &= P_{nd}(n) \times P_d(1) \times P_s(n+1) \\ &= C_n^{n+1} (1-\eta)^n \times \eta \times P_s(n+1), \end{aligned} \quad (9)$$

where C_n^{n+1} is the binomial coefficient, $P_d(n)$ [$P_{nd}(n)$] denotes the probability of detecting [not detecting] n photons. We find that $T_B \approx 0.5 \mu\text{s}$ remains optimal after taking this into account. Fig. 3d shows the rate of LC generation for $n = 1$ to 4 for different detector efficiencies.

To demonstrate the robustness of our protocol against nuclear environment fluctuations, we calculate the fidelity between the state obtained with and without Overhauser field (both for the the same set of precession phases determined by randomly chosen scattering times). For a pure hh, only the B_N^z Overhauser component perpendicular that is perpendicular to the applied B -field affects the protocol [by randomly modifying direction and magnitude of the total B -field by $\arctan(B_N^z/B_{ext})$]. By contrast, a mixed hh–lh system suffers predominantly from the parallel B_N^x component, to an extent determined by the mixing factor α . This is also exemplified in a decreased spin coherence time from the ideal hh limit, as shown in Fig. 3b. Only considering this term, the following analytical expression (see Appendix Sec E) captures the fidelity decay as a function of T_B :

$$\bar{\mathcal{F}}^{(1)} = \frac{1}{2} + \frac{\sqrt{2\pi}}{4T_B\delta B_N^x} \text{erf}\left(\frac{T_B\delta B_N^x}{\sqrt{2}}\right), \quad (10)$$

where $\bar{\mathcal{F}}^{(n)}$ denotes the average fidelity for a state of n scattered photons. For a single scattered photon, we obtain $\bar{\mathcal{F}}_{av}^{(1)} \rightarrow 1/2$ for large T_B as expected. More generally, Eqn. (10) represents an upper bound on the maximally achievable fidelity in the case of finite hh–lh mixing. To fully account for the effects of the stochastically varying net B -field vector, we show numerically obtained⁴⁹ fidelity overlaps of desired vs the ensemble-average of realised LC_4 states in Fig. 4. In the presence of the Overhauser field with fluctuations $\sim 14\text{mT}$, near unit fidelity remains possible in the region with (moderately) strong magnetic field $B \gtrsim 0.4 \text{ T}$ and relatively short $T_B \lesssim 0.25 \mu\text{s}$ (Fig. 4a). Conversely, large LC generation rates demand $0.5 \mu\text{s} \lesssim T_B \lesssim 1 \mu\text{s}$ and $B \lesssim 0.1 \text{ T}$ (Fig. 4b), so that a trade-off situation arises. Encouragingly, there is a wide middle-ground where high fidelity operation is possible at respectable rates.

Another important figure of merit of our protocol is the localisable entanglement (LE)^{13,50} between any two qubits of the LC state (and also the spin). The LE represents the maximum negativity of the reduced density matrix of two qubits of interest (indexed j and k), after all others have measured out projectively. Choosing the set of projectors $\mathcal{M} = \{P_i : 1 \leq i \leq n, i \notin \{j, k\}\}$ as our measurement defines an ensemble $\mathcal{E}_{\mathcal{M}} := \{p_{\mathcal{M},s}, \rho_{\mathcal{M},s}^{j,k}\}$, where $p_{\mathcal{M},s}$ is the probability of obtaining the two-spin density matrix $\rho_{\mathcal{M},s}^{j,k}$ for the outcome $\{s\}$ having measured the remaining $N-2$ qubits. The LE is then defined as the maximum negativity after averaging over all the

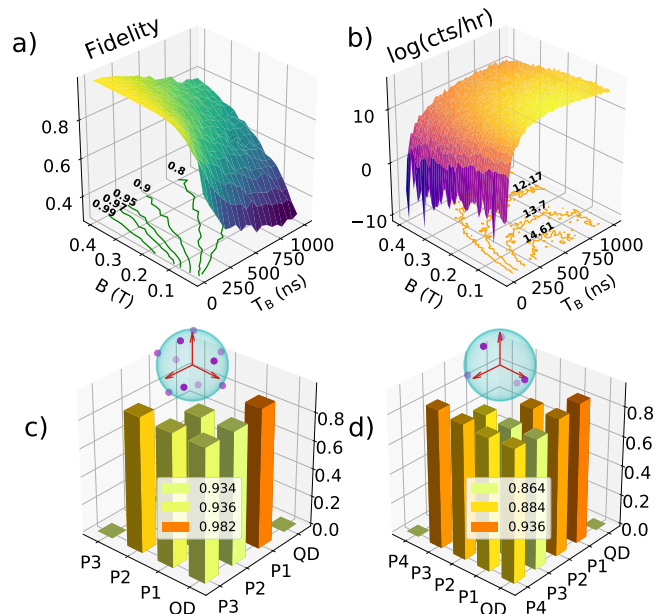


FIG. 4: **a)** Fidelity of the LC_4 state in the presence of the Overhauser field against applied field magnitude and single time-bin duration for a mixed hh–lh spin state. Overhauser fluctuations were 14 mT^{23} , with $g_h^x = 0.1$, $\alpha = .01$ and a completely unpolarised spin bath. **b)** Log of the success counts for a string of four photons. The overall detector efficiency was taken to be $\eta = 1$. The count rate increases with T_B until probability of multiple events in a single bin becomes significant. An increasing B-field decreases the count rate as predicted from Eqn. (8). **c and d)** Normalised LE for between pairwise combinations of a spin and 3 (panel c) or 4 (panel d) scattered photons, respectively. Due to computational constraints, we limited ourselves to ten (panel c) and five (panel d) uniformly distributed basis states on the Bloch sphere (with projectors shown in relevant insets).

outcomes for each measurement, that is

$$LE_{j,k}^N = \max_{\mathcal{M}} \sum_s p_{\mathcal{M},s} \mathcal{N}(\rho_{\mathcal{M},s}^{j,k}), \quad (11)$$

where $\mathcal{N}(\rho_{\mathcal{M},s}^{j,k})$ is the negativity of $\rho_{\mathcal{M},s}^{j,k}$. We choose a quasi-uniformly distributed basis on the Bloch sphere of each qubit (see points in insets of Fig. 4c,d). The computational unwieldiness of Eqn. (11) restricts the number of projectors, and we can only obtain a lower-bound of the true LE for LC_3 and LC_4 (Fig. 4c,d). Within the variance of the sample over which the optimisation was performed, the LE falls off with qubit distance, but encouragingly it remains remarkably high overall, and is thus unlikely to be a limiting factor in the length of the LC that could be generated using this protocol.

Conclusion – We have presented a novel scheme for generating frequency-encoded linear cluster states, which could serve as a stepping stone towards measurement-

based quantum computation. Unlike current rival schemes, our protocol does not rely on incoherent photon emission, and is therefore only sensitive to ground-state hole-spin dephasing, at the cost of being limited by its intrinsic probabilistic nature. Based on experimentally informed properties of real epitaxial quantum dots, we have shown that linear cluster states of sufficient length and high fidelity for fusion into larger cluster states can nevertheless be produced at respectable rates. Our protocol takes full account of unmitigated Overhauser field fluctuations. It is inherently impervious to hole-mixing induced modifications of the optical selection rules, but, like other approaches, it stands to gain from dynamic decoupling. Whilst the probabilistic nature of the Raman scattering events limits our protocol as described in the main text to LC states of length $n < 10$, our approach can, in principle, be made deterministic if embedded in a QD molecule, as discussed in Appendix Sec G. We believe such a Raman hole-spin emitter is a viable, practical alternative in the quest for realising non-classical multi-photon states, and importantly one which can be straightforwardly implemented with current expertise and devices.

Acknowledgments

We thank David Gershoni, Emil Denning, and Jake Iles-Smith for insightful and stimulating discussions. D.S. thanks SUPA for financial support. We acknowledge support from EPSRC (EP/M013472/01) and the ERC (no. 307392). B. D. G. thanks the Royal Society for a Wolfson Merit Award, and E. M. G. acknowledges support from the Royal Society of Edinburgh and the Scottish Government.

Appendix

A. Second-order perturbation rate

It can be easily shown that, after moving to a rotating frame with respect to the unperturbed transition frequency, the amplitude of the Raman-flip transition $|\downarrow\rangle \rightarrow |\uparrow\rangle$ is given by

$$\begin{aligned} \mathcal{T}_{\downarrow \rightarrow \uparrow} = & \frac{\langle \uparrow; \omega_R | H_I | T_{\downarrow}; 0 \rangle \langle T_{\downarrow}; 0 | H_I | \downarrow; \omega_{Ray} \rangle}{\hbar \Delta_1^{(1)}} \\ & + \frac{\langle \uparrow; \omega_{Ray} | H_I | T_{\uparrow}; 0 \rangle \langle T_{\uparrow}; 0 | H_I | \downarrow; \omega_B \rangle}{\hbar \Delta_2^{(1)}}, \end{aligned} \quad (\text{A1})$$

where $\Delta_1^{(1)} = \delta_h + \delta_e$, $\Delta_2^{(1)} = \delta_h - \delta_e$, and ω_R , ω_B and ω_{Ray} are the red-, blue-detuned and Rayleigh scattered photon frequencies, respectively. The first term in Eqn. (A1) gives the amplitude of a red Raman photon event: the system, initially in the $|\downarrow\rangle$ state, scatters a σ^V photon, after which the final state is given by $|\uparrow; H\rangle$ (that is, the system in the $|\uparrow\rangle$ state and a red-detuned Raman photon (σ^H polarised) is scattered). Similarly, the $|\uparrow\rangle \rightarrow |\downarrow\rangle$ transition giving rise to the blue-detuned photon scattering event occurs with amplitude

$$\begin{aligned} \mathcal{T}_{\uparrow \rightarrow \downarrow} = & \frac{\langle \downarrow; \omega_B | H_I | T_{\uparrow}; 0 \rangle \langle T_{\uparrow}; 0 | H_I | \uparrow; \omega_{Ray} \rangle}{\hbar \Delta_1^{(2)}} \\ & + \frac{\langle \downarrow; \omega_{Ray} | H_I | T_{\downarrow}; 0 \rangle \langle T_{\downarrow}; 0 | H_I | \uparrow; \omega_R \rangle}{\hbar \Delta_2^{(2)}}, \end{aligned} \quad (\text{A2})$$

where $\Delta_1^{(2)} = -\delta_h - \delta_e$, $\Delta_2^{(2)} = -\delta_h + \delta_e$.

The second term in each of the transition amplitudes does not contribute to the Raman processes, and vanish as the driving field can only drive vertically-polarised transitions. After performing the necessary solid angle integrals, we arrive at the scattering rate given by Eqn. (8) in the main text.

B. Overhauser field for hole-spin systems

Vanishing wavefunctions at the nuclear sites means that the Fermi-contact hyperfine term for the nuclear-hole spin interaction is effectively zero, leaving only the dipole-dipole interaction term as the dominant source of dephasing. For an idealised pure hh, this term is of Ising-nature, with just the ZZ component being present. In most epitaxially grown QDs, however, some degree of hh $|J; J_z\rangle = |3/2; \pm 3/2\rangle$ and lh $|J; J_z\rangle = |3/2; \pm 1/2\rangle$ mixing is always present^{21,51}, breaking the Ising-like nature of the dipole-dipole term and introducing XX and YY terms in the Hamiltonian. This means that the eigenstates of the Hamiltonian are no longer given separately by the hh or lh states, but a linear combination of both

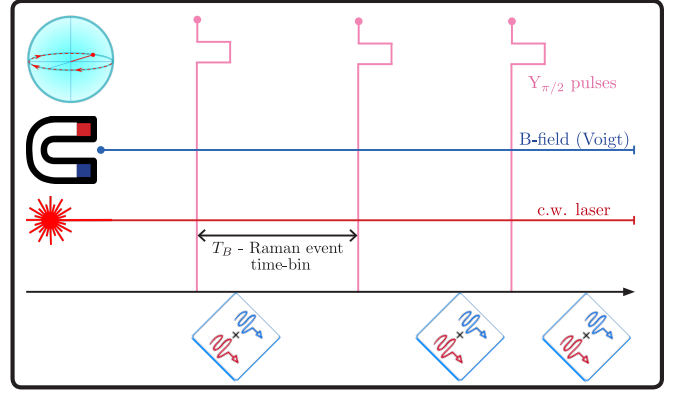


FIG. 5: Schematic representation of our protocol. The spin precesses in a constant magnetic field in Voigt geometry. Driven weakly and off-resonantly, the hole-spin scatters Raman-detuned photons at random intervals. The timing between Y-pulses T_B should be chosen so as to maximise the probability of getting a single scattering event between the pulses.

(the consequences of this mixing in quantum dot-based LC protocols is further discussed in Appendix Sec F). Without going into too much detail, the hyperfine coupling Hamiltonian for the hh-lh states is given by:

$$H_{hf}^{dd} = V \sum_j C_j |\Psi(\mathbf{R}_j)|^2 [\alpha(I_x^j S_x + I_y^j S_y) + I_z^j S_z] \quad (\text{B1})$$

where C_j are dipole-dipole hyperfine constants, V is the unit cell volume, and $\alpha = \frac{2}{\sqrt{3}}|\beta|$ is a parameter depending on the deformation potentials for the valence band, and the strain tensor^{21,51}. In the ‘frozen-fluctuation’ model²⁴, this results in an effective magnetic field with mean $\langle \mathbf{B}_N \rangle = (\langle B_N^x \rangle, \langle B_N^y \rangle, \langle B_N^z \rangle)$ (which, due to the finite size of the spin bath, is not necessarily zero), and a fluctuation $\delta \mathbf{B}_N = (\delta B_N^x, \delta B_N^y, \delta B_N^z)$ (which is the source of the spin’s loss of coherence), and is assumed to follow normal statistics²¹:

$$\begin{aligned} P(\mathbf{B}_N) = & \left(\frac{1}{2\pi} \right)^{\frac{3}{2}} \frac{1}{\delta B_N^{\parallel 2} \delta B_N^{\perp 2}} \\ & \times \exp \left[-\frac{\Delta B_N^{x 2}}{2 \delta B_N^{\parallel 2}} - \frac{\Delta B_N^{y 2}}{2 \delta B_N^{\parallel 2}} - \frac{\Delta B_N^{z 2}}{2 \delta B_N^{\perp 2}} \right], \end{aligned} \quad (\text{B2})$$

where $\Delta B_N^i = B_N^i - \langle B_N^i \rangle$, $\delta B_N^{\perp} = \delta B_N^z$ and $\delta B_N^{\parallel} := \delta B_N^x = \delta B_N^y = \alpha \delta B_N^{\perp}$. Experimentally, Overhauser field fluctuations of 10-30mT have been measured^{26,27}, putting a lower-bound on the applied external field required to screen these fluctuations.

C. Matrix operations

Consider a single scattering process that can be described by the action of the product of matrices:

$$\begin{aligned} |\uparrow\rangle |Ray_k\rangle &\rightarrow e^{-i\frac{\phi_1^{(k)}}{2}} e^{i\frac{\phi_2^{(k)}}{2}} (|\uparrow\rangle + |\downarrow\rangle) |B_k\rangle \\ &= U_r U_p(\phi_2^{(k)}) T_s^{(k)} U_p(\phi_1^{(k)}) |\uparrow\rangle |Ray_k\rangle \\ &= Q^{(k)} |\uparrow\rangle |Ray_k\rangle , \end{aligned} \quad (C1)$$

$$\begin{aligned} |\downarrow\rangle |Ray_k\rangle &\rightarrow e^{i\frac{\phi_1^{(k)}}{2}} e^{-i\frac{\phi_2^{(k)}}{2}} (|\uparrow\rangle - |\downarrow\rangle) |R_k\rangle \\ &= U_r U_p(\phi_2^{(k)}) T_s^{(k)} U_p(\phi_1^{(k)}) |\downarrow\rangle |Ray_k\rangle \\ &= Q^{(k)} |\downarrow\rangle |Ray_k\rangle , \end{aligned}$$

where $U_p(\phi_{1,2}^{(k)})$ is the free spin precession transformation before ($\phi_1^{(k)}$) and after ($\phi_2^{(k)}$) the k^{th} scattering event (prior to the $Y_{\frac{\pi}{2}}$ rotation), with the resulting matrix of events being $Q^{(k)} := U_r U_p(\phi_2^{(k)}) T_s^{(k)} U_p(\phi_1^{(k)})$. The scattering matrix $T_s^{(k)}$ is given by

$$T_s^{(k)} = \left(\begin{array}{c|c} 0 & T_R^{(k)} \\ \hline T_B^{(k)} & 0 \end{array} \right) , \quad (C2)$$

with $T_R^{(k)}$ and $T_B^{(k)}$ written in the basis $\{|B_k\rangle, |R_k\rangle, |Ray_k\rangle\}$, which simultaneously flips the spin state $|\uparrow\rangle \leftrightarrow |\downarrow\rangle$, and applies the local transformations

$$\begin{aligned} T_B^{(k)} : |Ray_k\rangle &\mapsto |B_k\rangle \\ T_R^{(k)} : |Ray_k\rangle &\mapsto |R_k\rangle , \end{aligned} \quad (C3)$$

where we have omitted the unaffected photon states for brevity. Hence $T_B^{(k)}$ and $T_R^{(k)}$ take the form:

$$\begin{aligned} T_R^{(k)} &= \mathbb{I}_3^{\otimes k-1} \otimes \begin{pmatrix} 0 & 0 & 0 \\ 0 & 0 & 1 \\ 0 & 0 & 0 \end{pmatrix} \otimes \mathbb{I}_3^{\otimes n-k} \\ T_B^{(k)} &= \mathbb{I}_3^{\otimes k-1} \otimes \begin{pmatrix} 0 & 0 & 1 \\ 0 & 0 & 0 \\ 0 & 0 & 0 \end{pmatrix} \otimes \mathbb{I}_3^{\otimes n-k} , \end{aligned} \quad (C4)$$

and U_r and $U_p(\phi)$ are simply given by given by

$$\begin{aligned} U_r &= \exp\left(i\frac{\pi}{4}\sigma_y\right) \otimes \mathbb{I}_3^{\otimes n} \\ U_p(\phi) &= \begin{pmatrix} e^{-i\frac{\phi}{2}} & 0 \\ 0 & e^{i\frac{\phi}{2}} \end{pmatrix} \otimes \mathbb{I}_3^{\otimes n} , \end{aligned} \quad (C5)$$

where the first matrices act on the spin state and have been written in the $\{|\uparrow\rangle, |\downarrow\rangle\}$ basis. Unfortunately, the matrix product describing n -photon scattering events becomes unwieldy with increasing n . In Appendix Sec D, however, we show that this protocol does indeed generalise to a LC_n state, up to free precession phases.

D. Generalisation to n -photons

1. Preliminary lemmas

In this section, we will show that the general form of the n -photon state $S^{(n)}$ obtained using our protocol can be written recursively. In fact,

Lemma D.1. $\forall n \in \mathbb{N}$, the n -photon state $S^{(n)}$ can be decomposed into the recursive relations

$$\begin{aligned} S_+^{(n)} &= S_+^{(n-1)} |1_n\rangle + S_-^{(n-1)} |0_n\rangle , \\ S_-^{(n)} &= S_+^{(n-1)} |1_n\rangle - S_-^{(n-1)} |0_n\rangle , \end{aligned} \quad (D1)$$

depending whether the spin is measured to be in the $|\uparrow\rangle$ or $|\downarrow\rangle$ state, respectively.

Proof. We will, w.l.o.g., ignore the spin precession, although the proof is the same for the general case:

Basis case: For $j = 1$, $S_+^{(1)} = |1_1\rangle + |0_1\rangle$ and $S_-^{(1)} = |1_1\rangle - |0_1\rangle$. After the next scattering event, we get

$$\begin{aligned} S_+^{(2)} &= |1_1 1_2\rangle + |1_1 0_2\rangle + |0_1 1_2\rangle - |0_1 0_2\rangle \\ &= (|1_1\rangle + |0_1\rangle) |1_2\rangle + (|1_1\rangle - |0_1\rangle) |0_2\rangle \\ &= S_+^{(1)} |1_2\rangle + S_-^{(1)} |0_2\rangle . \end{aligned} \quad (D2)$$

Similarly,

$$\begin{aligned} S_-^{(2)} &= |1_1 1_2\rangle - |1_1 0_2\rangle + |0_1 1_2\rangle + |0_1 0_2\rangle \\ &= (|1_1\rangle + |0_1\rangle) |1_2\rangle - (|1_1\rangle - |0_1\rangle) |0_2\rangle \\ &= S_+^{(1)} |1_2\rangle - S_-^{(1)} |0_2\rangle . \end{aligned} \quad (D3)$$

Induction step: Assume statement holds for $j = n$, and consider the $(n+1)^{\text{th}}$ scattering event:

$$\begin{aligned} S_+^{(n+1)} &= U_r T_{scat}^{(n+1)} (|\uparrow\rangle S_+^{(n)} + |\downarrow\rangle S_-^{(n)}) |Ray_{n+1}\rangle \\ &= (|\uparrow\rangle + |\downarrow\rangle) S_+^{(n)} |1_{n+1}\rangle + (|\uparrow\rangle - |\downarrow\rangle) S_-^{(n)} |0_{n+1}\rangle \\ &= |\uparrow\rangle (S_+^{(n)} |1_{n+1}\rangle + S_-^{(n)} |0_{n+1}\rangle) \\ &\quad + |\downarrow\rangle (S_+^{(n)} |1_{n+1}\rangle - S_-^{(n)} |0_{n+1}\rangle) . \end{aligned} \quad (D4)$$

Therefore $S_+^{(n+1)} = S_+^{(n)} |1_{n+1}\rangle + S_-^{(n)} |0_{n+1}\rangle$ and $S_-^{(n+1)} = S_+^{(n)} |1_{n+1}\rangle - S_-^{(n)} |0_{n+1}\rangle$, so the statement holds $\forall n \in \mathbb{N}$. ■

It is then easy to see that we also have that

Lemma D.2.

$$\sigma_z^{(n)} S_{\pm}^{(n)} = -S_{\mp}^{(n)} \quad \forall n \in \mathbb{N}, \quad (\text{D5})$$

which we shall use to prove that the n -photon state we generate is indeed a linear cluster state.

2. Equivalence to LC_n states

In order to show that the $S_{\pm}^{(n)}$ states are indeed LC_n s, we have to show that they both satisfy the set of eigenvalue equations

$$K_n^{(a)} S_{\pm}^{(n)} = (-1)^{k_{\pm}^{(a)}} S_{\pm}^{(n)}, \quad (\text{D6})$$

with

$$K_n^{(a)} = \sigma_x^{(a)} \bigotimes_{b \in N(a)} \sigma_z^{(b)}, \quad (\text{D7})$$

where $1 \leq a \leq n$, $N(a)$ is the set of direct neighbours of photon a along the state, and $k_{\pm}^{(a)} \in \{0, 1\}$, depending on the particular realisation of LC_n . The subscript on the operator K denotes the state tensor-length of K , and hence the length of the state it acts upon. In fact we shall show the following statement

Theorem D.3. *The n -photon $S^{(n)}$ state satisfies the set of LC_n -eigenvalue equations for*

$$\begin{aligned} k_+^{(a)} &= \begin{cases} 1, & \text{if } a \in \{1, n\} \\ 0, & \text{if } 1 < a < n \end{cases} \\ k_-^{(a)} &= \begin{cases} 1, & \text{if } a = 1 \\ 0, & \text{if } 1 < a \leq n \end{cases} \end{aligned} \quad (\text{D8})$$

Proof. The proof follows, once again, by induction, as well as the use of Lemma D.1

Basis case: For $j = 2$,

$$\begin{aligned} S_+^{(2)} &= (|1_1\rangle + |0_2\rangle) |1_n\rangle + (|1_1\rangle - |0_1\rangle) |0_2\rangle, \\ S_+^{(2)} &= (|1_1\rangle + |0_2\rangle) |1_n\rangle - (|1_1\rangle - |0_1\rangle) |0_2\rangle, \end{aligned} \quad (\text{D9})$$

and the statement holds when applying $\sigma_x^{(1)} \otimes \sigma_z^{(2)}$ and $\sigma_z^{(1)} \otimes \sigma_x^{(2)}$.

Induction step: Suppose the statement holds for $j = n$, and consider $S_+^{(n+1)} = S_+^{(n)} |1_{n+1}\rangle + S_-^{(n)} |0_{n+1}\rangle$. Then

If $a = 1$:

$$\begin{aligned} K_{n+1}^{(a)} S_+^{(n+1)} &= (K_n^{(a)} \otimes \mathbb{I}_2)(S_+^{(n)} |1_{n+1}\rangle + S_-^{(n)} |0_{n+1}\rangle) \\ &= (-1)^{k_+^{(1)}} S_+^{(n)} |1_{n+1}\rangle + (-1)^{k_-^{(1)}} S_-^{(n)} |0_{n+1}\rangle \\ &= -(S_+^{(n)} |1_{n+1}\rangle + S_-^{(n)} |0_{n+1}\rangle) \\ &= -S_+^{(n+1)}, \end{aligned} \quad (\text{D10})$$

with \mathbb{I}_2 being the 2×2 identity matrix. The penultimate step holds due the induction hypothesis. Similarly, for $S_-^{(n+1)}$,

$$\begin{aligned} K_{n+1}^{(a)} S_-^{(n+1)} &= (K_n^{(a)} \otimes \mathbb{I}_2)(S_+^{(n)} |1_{n+1}\rangle - S_-^{(n)} |0_{n+1}\rangle) \\ &= (-1)^{k_+^{(1)}} S_-^{(n)} |1_{n+1}\rangle - (-1)^{k_-^{(1)}} S_-^{(n)} |0_{n+1}\rangle \\ &= -(S_+^{(n)} |1_{n+1}\rangle - S_-^{(n)} |0_{n+1}\rangle) \\ &= -S_-^{(n+1)}. \end{aligned} \quad (\text{D11})$$

If $1 < a < n$:

$$\begin{aligned} K_{n+1}^{(a)} S_+^{(n+1)} &= (K_n^{(a)} \otimes \mathbb{I}_2)(S_+^{(n)} |1_{n+1}\rangle + S_-^{(n)} |0_{n+1}\rangle) \\ &= (-1)^{k_+^{(a)}} S_+^{(n)} |1_{n+1}\rangle + (-1)^{k_-^{(a)}} S_-^{(n)} |0_{n+1}\rangle \\ &= S_+^{(n)} |1_{n+1}\rangle + S_-^{(n)} |0_{n+1}\rangle \\ &= S_+^{(n+1)}, \end{aligned} \quad (\text{D12})$$

$$\begin{aligned} K_{n+1}^{(a)} S_-^{(n+1)} &= (K_n^{(a)} \otimes \mathbb{I}_2)(S_+^{(n)} |1_{n+1}\rangle - S_-^{(n)} |0_{n+1}\rangle) \\ &= (-1)^{k_+^{(a)}} S_-^{(n)} |1_{n+1}\rangle - (-1)^{k_-^{(a)}} S_-^{(n)} |0_{n+1}\rangle \\ &= S_+^{(n)} |1_{n+1}\rangle - S_-^{(n)} |0_{n+1}\rangle \\ &= S_-^{(n+1)}. \end{aligned} \quad (\text{D13})$$

If $a = n$:

$$\begin{aligned} K_{n+1}^{(a)} S_+^{(n+1)} &= (K_n^{(a)} \otimes \sigma_z^{(n+1)})(S_+^{(n)} |1_{n+1}\rangle + S_-^{(n)} |0_{n+1}\rangle) \\ &= -(-1)^{k_+^{(n)}} S_+^{(n)} |1_{n+1}\rangle + (-1)^{k_-^{(n)}} S_-^{(n)} |0_{n+1}\rangle \\ &= S_+^{(n)} |1_{n+1}\rangle + S_-^{(n)} |0_{n+1}\rangle \\ &= S_+^{(n+1)}, \end{aligned} \quad (\text{D14})$$

$$\begin{aligned}
K_{n+1}^{(a)} S_-^{(n+1)} &= (K_n^{(a)} \otimes \sigma_z^{(n+1)})(S_+^{(n)} |1_{n+1}\rangle - S_-^{(n)} |0_{n+1}\rangle) \\
&= -(-1)^{k_+^{(n)}} S_-^{(n)} |1_{n+1}\rangle - (-1)^{k_-^{(n)}} S_-^{(n)} |0_{n+1}\rangle \\
&= S_+^{(n)} |1_{n+1}\rangle - S_-^{(n)} |0_{n+1}\rangle \\
&= S_-^{(n+1)}.
\end{aligned} \tag{D15}$$

For the $a = n+1$ case, we shall make use of Lemma D.2. The operator $K_{n+1}^{(n+1)}$ can be decomposed as $\mathbb{I}_2^{\otimes n-1} \otimes \sigma_z^{(n)} \otimes \sigma_x^{(n+1)}$, and hence we get that

If $a = n + 1$:

$$\begin{aligned}
K_{n+1}^{(a)} S_+^{(n+1)} &= -S_-^{(n)} |0_{n+1}\rangle - S_+^{(n)} |1_{n+1}\rangle \\
&= -S_+^{(n+1)},
\end{aligned} \tag{D16}$$

$$\begin{aligned}
K_{n+1}^{(a)} S_-^{(n+1)} &= -S_-^{(n)} |0_{n+1}\rangle + S_+^{(n)} |1_{n+1}\rangle \\
&= S_-^{(n+1)}.
\end{aligned} \tag{D17}$$

Therefore, the states $S_{\pm}^{(n)}$ satisfy the eigenvalue conditions (D6) for the set of parameters (D8), meaning that the the state obtained by our protocol is an LC_n state. ■

E. Average fidelity

Consider a single scattering event in which the spin precesses for a time $T_B^{(1)}$ prior to the scattering event and a subsequent precession time $T_B^{(2)}$ followed by a Y rotation marking the end of the run (such that $T_B^{(1)} + T_B^{(2)} = T_B$). In the presence of the B_N^x component, the rotation matrix $U_p(\phi)$ in (C5) picks up a stochastic term $\omega_N t$, that is

$$U_p((\omega_B + \omega_N)t) = \begin{pmatrix} e^{-i\frac{1}{2}(\omega_B + \omega_N)t} & 0 \\ 0 & e^{i\frac{1}{2}(\omega_B + \omega_N)t} \end{pmatrix} \otimes \mathbb{I}_3^{\otimes n}, \tag{E1}$$

with $t = T_B^{(1)}$ or $T_B^{(2)}$, where we have written the precessed angle explicitly in terms of $\omega_B = g_h^x \mu_B B_{ext} / \hbar$ and the Overhauser stochastic frequency $\omega_N = g_h^x \mu_B B_N^x / \hbar$ (g_h^x being the x component of the anisotropic hole g-factor⁵²).

The effect of this stochastic term can be seen in the trace fidelity between post Y rotation ideal photon state, and the more realistic case including the Overhauser field. The spin+photon states for the two cases, denoted by $S^{(1)}$ and $\tilde{S}^{(1)}$, respectively, are then given by

$$\begin{aligned}
S^{(1)} &= e^{-i\frac{1}{2}\omega_B \delta T_B} |\uparrow B_1\rangle + e^{-i\frac{1}{2}\omega_B \delta T_B} |\downarrow B_1\rangle \\
&\quad + e^{i\frac{1}{2}\omega_B \delta T_B} |\uparrow R_1\rangle - e^{i\frac{1}{2}\omega_B \delta T_B} |\downarrow R_1\rangle, \\
\tilde{S}^{(1)} &= e^{-i\frac{1}{2}(\omega_B + \omega_N) \delta T_B} |\uparrow B_1\rangle + e^{-i\frac{1}{2}(\omega_B + \omega_N) \delta T_B} |\downarrow B_1\rangle \\
&\quad + e^{i\frac{1}{2}(\omega_B + \omega_N) \delta T_B} |\uparrow R_1\rangle - e^{i\frac{1}{2}(\omega_B + \omega_N) \delta T_B} |\downarrow R_1\rangle,
\end{aligned} \tag{E2}$$

where $\delta T_B = T_B^{(1)} - T_B^{(2)} \in [-T_B, T_B]$ is a uniform random variable due to the fact that the spin precesses multiple times during T_B in the high external magnetic field. The final photon state, as discussed earlier, depends on the state the spin is measured in, so we shall denote the density matrices of the ideal and realistic cases by $\rho_+^{(1)}$ and $\xi_+^{(1)}$, respectively, if the spin is measured in the $|\uparrow\rangle$ state, and similarly $\rho_-^{(1)}$ and $\xi_-^{(1)}$ for the $|\downarrow\rangle$ result. The fidelity for a fixed value of B_N^x is then given by $\mathcal{F}^{(1)} = \text{tr}(\rho_+^{(1)} \xi_+^{(1)}) = \text{tr}(\rho_-^{(1)} \xi_-^{(1)}) = \cos^2(B_N^x \delta T_B / 2)$.

Due to the stochastic nature of the Overhauser field, we need to ensemble-average $\mathcal{F}^{(1)}$ in order to get the true fidelity, that is $\bar{\mathcal{F}}^{(1)} = \left\langle \left\langle \text{tr}(\rho_-^{(1)} \xi_-^{(1)}) \right\rangle_B \right\rangle_{\delta T} = \left\langle \left\langle \text{tr}(\rho_+^{(1)} \xi_+^{(1)}) \right\rangle_B \right\rangle_{\delta T}$, where the Overhauser averaging $\langle \cdot \rangle_B$ and time averaging $\langle \cdot \rangle_{\delta T}$ are performed over a normal distribution with zero mean and finite standard deviation δB_N^x , and a uniform distribution over $[-T_B, T_B]$ ⁵³. In doing so, we get the averaged fidelity for a single scattering event in the presence of B_N^x given by Eqn. 10.

F. Imperfections of other QD-based protocols

As discussed in the main text, several protocols have been proposed for implementing photonic LC states or entangled states sharing similar properties. The influential 2009 proposal by Lindner and Rudolph⁹ (LR) offered an elegant and simple scheme which could be implemented using the circularly polarised degrees of freedom of a quantum dot. Despite its simplicity, a number of experimental barriers need to be overcome to actually implement such a scheme. We discuss these below both for the LR scheme as well as the recent dark exciton (DE) based LC scheme¹³, which has already successfully produced LC_2 states in the laboratory and shown promise for reaching up to LC_5 . In essence, these imperfections effectively introduce a limits to the size of achievable cluster states for those protocols, and preclude indefinite deterministic operation. By contrast, we note that our approach in this work – as discussed in the main paper – is largely immune against all issues discussed below.

1. Overhauser field limitations

The relatively short T_2^* time of the electron spin due to the fluctuating nuclear environment constitutes a severe shortcoming of real quantum dot spins, putting a limit on the order of a few nanoseconds on any experiment relying on the coherence of this system. For the LR protocol⁹ one requires an external field of the order of $\sim 50\text{mT}$ along the Y direction in order to obtain a sufficient number of Y-gates for a multi photon $\text{LC}_{4 \geq n \geq 2}$ state within a few nanoseconds (assuming instantaneous excitation and radiative decay). Such an applied field, however, activates the previously dipole-forbidden transitions, degrading the correlations between the spin and emitted photons required for the LC state. Applying a strong field results in significant electron-spin precession between the pulsed excitation and spontaneous emission events, reducing the fidelity of the produced LC. By contrast, applying a weaker field limits the scalability of the protocol beyond a string of a couple of photons, as well as failing to screen the effects of the fluctuating Overhauser field. In short, the presence of the Overhauser field implies that the LR protocol would in practice need to be upgraded to incorporate dynamical decoupling and gated Y-rotations instead of relying on free spin precession.

One way to overcome some of these hurdles would be to adapt the LR protocol to a hole-spin system, having a longer dephasing time. However, due to the hole spins coupling weakly to external magnetic fields, the precession time would be much longer, requiring stronger fields to implement the Y-rotations, hence resulting in the same issue discussed above; namely, the undesirable dipole-forbidden transitions becoming accessible. Shorter coherence times in the presence of a weak external field and phonon sideband emissions (see below) would also be an issue in the hole-spin variant of the LR scheme.

Extending the promising dark exciton (DE) scheme¹³ beyond a couple of photons present similar experimental challenges: the finite radiative lifetime of the biexciton (BiE) $\tau_{\text{BiE}} \approx 0.33\text{ns}$ entails that the spin precesses by a non-negligible random amount both in the DE and BiE states, and this limits the purity of the photon polarisation state. Furthermore, the DE spin also suffers from environmental decoherence during its precession¹³.

2. Shortcomings due to coupling to phonons

The solid-state environment further limits the deterministic nature of these protocols due to coupling to the phonon environment. Even in the limit of idealised instantaneous excitation pulses, a temperature-dependent fraction of the photons are inevitably emitted incoherently via the phonon sideband ($\sim 9\%$ at temperatures as low as $T = 4\text{K}$, increasing with temperature⁵⁴). This affects all protocols involving electronic excitation to trion or biexciton states, i.e. both the LR and DE approaches.

3. Effects of hole state mixing

In this section, we discuss how said protocols fare against finite hh-lh mixing⁵⁵. The first type of hh-lh mixing, due to anisotropy in the in-plane strain of the quantum dot, gives rise to the $\text{hh}\uparrow\text{-lh}\downarrow$ mixing, resulting in the hole eigenstates

$$\begin{aligned} |\uparrow\rangle &= \frac{1}{\sqrt{1 + |\beta_{ud}|^2}} (|3/2; +3/2\rangle + \beta_{ud} |3/2; -1/2\rangle), \\ |\downarrow\rangle &= \frac{1}{\sqrt{1 + |\beta_{ud}|^2}} (|3/2; -3/2\rangle + \beta_{ud}^* |3/2; +1/2\rangle), \end{aligned} \quad (\text{F1})$$

where, without giving its explicit form, β_{ud} is the in-plane strain-dependent mixing factor^{21,51}. This type of mixing primarily causes ellipticity of the dipole-allowed transitions which, for a hh system, would be driven by σ^\pm polarized light. Hence this $\text{hh}\uparrow\text{-lh}\downarrow$ mixing does not induce the ‘diagonal’ dipole-forbidden transitions.

On the other hand, the $\text{hh}\uparrow\text{-lh}\uparrow$ mixing may allow transitions which would otherwise be forbidden for a hh system. The hole eigenstates solely due this type of mixing are given by:

$$\begin{aligned} |\uparrow\rangle &= \frac{1}{\sqrt{1 + |\beta_{uu}|^2}} (|3/2; +3/2\rangle + \beta_{uu} |3/2; +1/2\rangle), \\ |\downarrow\rangle &= \frac{1}{\sqrt{1 + |\beta_{uu}|^2}} (|3/2; -3/2\rangle + \beta_{uu}^* |3/2; -1/2\rangle), \end{aligned} \quad (\text{F2})$$

where β_{uu} is the $\text{hh}\uparrow\text{-lh}\uparrow$ admixture factor^{21,51}. From Eqns. (F2), it can be immediately seen that the transitions, which are forbidden in Faraday geometry, are now allowed. For hole-spins, β_{uu} has been measured to be $\sim 8\%$, leading to allowed-to-forbidden transition ratios of $|\beta_{uu}|^2/3 \approx 0.2\%$ ⁵¹, although this varies from one quantum dot to another. This means that even if the external field in the LR scheme is weak enough to preserve a pure Faraday geometry, dipole-forbidden transitions may still occur with some small, but finite probability, both for the original and the hole-spin variant of the LR protocol.

Similarly, in the DE system z -polarised ‘forbidden’ transitions are also present due to hole sub-band mixing, although these transitions in this system are significantly weaker^{56,57}. In addition to hh-lh mixing, the DE scheme also suffers from dark-bright exciton (DE-BE) state mixing due to the breaking of the C_{2v} symmetry, although this effect is much weaker than the hh-lh mixing. Realistically, self-assembled QDs suffer from a reduction in symmetry during the growth process, causing a departure from the ideal C_{2v} symmetry. The resulting ‘reduced’ C_s symmetry leads to DE-BE state couplings of two kinds; the first leads to finite z -polarised dipole transitions similar to the $\text{hh}\uparrow\text{-lh}\downarrow$ admixture in the BE schemes, whilst the second gives rise to forbidden in-plane transitions, bearing similar repercussions as the $\text{hh}\uparrow\text{-lh}\uparrow$ mixing dis-

cussed above^{56,58}.

We note that our approach does not suffer from modifications of the selection rules due to hole mixing: we already rely on the presence of off-diagonal transitions and slight changes to their rates will not make an appreciable difference.

4. Robustness of 2D cluster state protocols

Schemes extending the LR scheme for 2D cluster state generation have been proposed¹⁷, in which it was shown that a pair of entangled QDs could be used to directly generate a 2D cluster state, reducing the required number of probabilistic fusion of LC state building blocks. Furthermore, it was recently shown that the requirement of two-qubit gates on the entangling emitters can be relaxed by a careful application of pulses and single-qubit gates on the emitters¹⁸. However, building on a similar setup and selection rules as the original LR protocol, we expect that the practical limitations discussed above will also limit the achievable size of photonic states that can be obtained with this protocol.

G. Proposal for deterministic scheme using DQD

The biggest drawback of our scheme is its apparently inherent probabilistic nature due to the random timings of the Raman scattering events. If we could learn when a Raman flip has occurred prior to detecting the emitted photon, we could apply the Y -rotations accordingly (i.e. after each Raman flip) and we would also know any local phases on our photons. The most elegant way of doing this would be to detect the presence of the Raman scattered photons without absorbing them or learning their frequency, however, this ability does not currently exist for optical photons, which is why we turn to observing the QD spin instead. Continuously monitoring whether a Raman spin-flip has happened, but without learning the spin state itself, requires the introduction of a secondary ‘ancilla’ quantum dot as a witness of the spin-photon entangling event.

Motivated by recent theoretical and experimental work, we propose extending our Raman protocol to a double quantum dot (DQD) system, where, depending on the relative strength of the exchange interaction and transition energy detuning between the two QDs, either joint measurements on the DQD system can be performed, whilst leaving the photon-entangling hole spin state unaffected, or oscillations between joint states can be detected without collapsing the system joint state. In the following, we will discuss two possibilities of extending our protocol in such a way.

A) Electrical control: During the past few years, great progress has been made in synthesising and controlling quantum dot molecules, both in stacked^{59–61} and lateral^{62,63} geometries. A Raman-spin flip DQD scheme

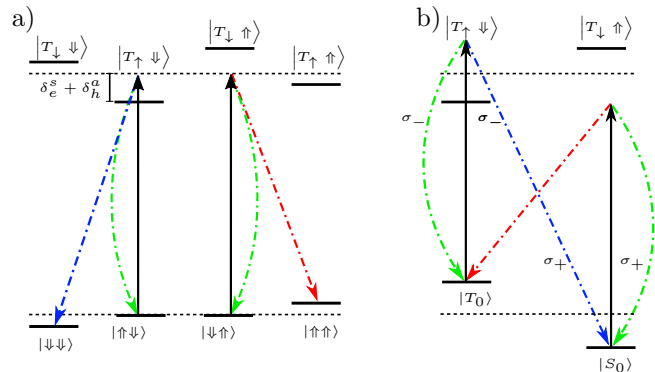


FIG. 6: **a)** Extending the Raman spin-flip protocol to a DQD setup in Voigt geometry, where the two QDs are sufficiently detuned (relative to the exchange interaction), allowing the optical addressing of a single spin. **b)** An alternative setup in Faraday geometry⁶⁴, in which the initial state would be a superposition of S and T_0 states.

was shown in Ref. 64, in which the external field is applied in Faraday geometry and the Raman spin-flips occur between the singlet S and triplet T_0 states of the system. Whilst this configuration would not allow screening of the dominant fluctuation component of the Overhauser field, such a setup would, in principle, allow a current measurement scheme to be applied and signal the Raman events. In fact, the standard singlet-triplet spin-blockade used in gated-DQDs⁶⁵ could be used to detect current drops, signalling the Raman event. This would require operation around the $(1,0),(1,1),(2,0)$ triple-point at a negative bias, making use of the additional charge state $S(2,0)$. Addressing and manipulation of these singlet and triplet states in optically-active DQDs have been recently demonstrated for QD molecules^{61,64,66–68}, whereas the current transport measurements has been long understood for surface-defined QDs. This route would require a hybrid gated and optically-active device, which, although certainly challenging, might nonetheless present a feasible route.

B) Optical control: A more attractive alternative to having a gated structure would be to have an all-optical non-invasive spin readout technique, provided by the rich energy level structure for these systems. In quantum dot molecules, this can be achieved by using the distributed trion state, with the ancilla spin being empty, whilst the host spin being singly-electron charged. The spin readout technique was demonstrated experimentally performing resonance fluorescence (RF) on the $|\downarrow_s, 0_a\rangle \leftrightarrow |\downarrow_s, \downarrow\uparrow_a\rangle$ transition, which is decoupled from the main spin-flip transition⁶⁹. This technique could be readily extended to hole spin systems with an analogous level structure. A similar setup was demonstrated experimentally in Ref. 70, where use of these cycling transitions was made to detect the flips of the host spin state. Both these setups would require individual addressing of the

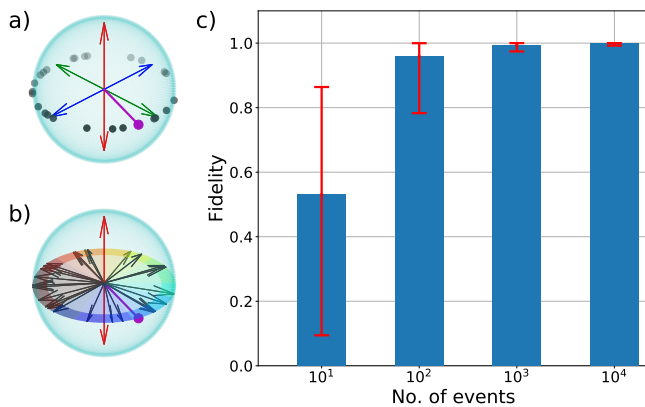


FIG. 7: **a)** Bloch sphere representation of the problem: the actual state to be reconstructed (purple) gains a random phase (dots) prior to every measurement, with the measurement bases given by the arrows. **b)** An equivalent picture where the state is fixed, with the ‘random’ measurement basis given by the phases. **c)** Fidelity for 16 grouped projectors, showing, as expected, an increase in the Fidelity for higher numbers of events.

ancilla and host spin, meaning that the two QDs selected must be sufficiently relatively far-detuned, which could be achieved by tuning the bias voltage over the sample, decreasing the exchange energy splitting⁶⁶. Alternatively, for samples with a much stronger singlet-triplet splitting, optical addressing of the joint states would be more feasible. In the singlet-triplet Raman scheme in Faraday geometry discussed in Ref. 64 (Fig. 6b), spin readout of the singlet state can be performed by using the decoupled cycling transition $T_+ \leftrightarrow R_{++}$ ⁶⁷.

H. Quantum state tomography

Quantum state tomography (QST) allows one to completely characterise an unknown quantum state, as long

as an ensemble of identical copies of such a state can be created in the experiment. Despite the wide range of tomographic techniques in existence^{71–73}, the aim is typically to use sets of repeated measurements on the ensemble, the results of which enable the reconstruction of the original state.

Our probabilistic protocol then presents an obvious question as to how would one obtain multiple copies of the cluster state, since for each realisation, the phases imprinted on the photonic qubits are random, and are only known post-detection. Using conventional reconstruction techniques would then average over the coherences of the cluster state, losing the entanglement information.

Despite this apparent downfall, the fact that the random phases can be determined post-measurement means that this problem can be reformulated in a ‘static frame’ with respect to the state, that is, the state is not imprinted with the phases, instead, in this frame, the effective basis chosen for the actual measurement rotates for each measurement due to the different phases. The problem then reduces to reconstructing a state when the measurement basis used is different for each measurement. We emphasise that this does not mean that the experimentally chosen basis is actually rotated for each measurement. The random measurement projectors can then be grouped as $\{P_1^{(j)}, P_1^{(j)}, \dots, P_{n_j}^{(j)}\}$ by proximity on the Bloch sphere into projectors $\{\mathcal{P}_j : 1 \leq j \leq K\}$ to be used for reconstruction.

As a proof of principle, we used the state $c_1 |H\rangle + c_2 |V\rangle$ for each experiment, where c_1 and c_2 are two random complex numbers, so that each time we have a different measurement projector. Using Maximum Likelihood Estimation (MLE) and the Cholesky decomposition for the density matrix, we performed QST for various numbers of grouped projectors, the results of which are shown in Fig. 7. As the number of \mathcal{P}_j is increased, the fidelity rises, as expected. However, for lower numbers of events, the fidelity peaks at a number of grouped projectors, and then starts declining again. This drop is due to the failure of the Gaussian assumption used for MLE. This failure is expected to affect fidelities for higher event numbers as we increase the number of projectors.

* ds32@hw.ac.uk

† e.gauger@hw.ac.uk

¹ Hans J. Briegel and Robert Raussendorf. Persistent entanglement in arrays of interacting particles. *Phys. Rev. Lett.*, 86:910–913, Jan 2001.

² Robert Raussendorf and Hans J. Briegel. A one-way quantum computer. *Phys. Rev. Lett.*, 86:5188–5191, May 2001.

³ R. Raussendorf, J. Harrington, and K. Goyal. Topological fault-tolerance in cluster state quantum computation. *New Journal of Physics*, 9(6):199, 2007.

⁴ Jeremy L. O’Brien, Akira Furusawa, and Jelena Vuckovic. Photonic quantum technologies. *Nat Photon*, 3(12):687–695, Dec 2009.

⁵ Daniel E. Browne and Terry Rudolph. Resource-efficient linear optical quantum computation. *Phys. Rev. Lett.*, 95:010501, Jun 2005.

⁶ David A. Herrera-Martí, Austin G. Fowler, David Jennings, and Terry Rudolph. Photonic implementation for the topological cluster-state quantum computer. *Phys. Rev. A*, 82:032332, Sep 2010.

⁷ Y.S. Weinstein. Fusing imperfect photonic cluster states. *Journal of Modern Optics*, 58(14):1285–1291, 2011.

⁸ Michael A. Nielsen. Optical quantum computation using cluster states. *Phys. Rev. Lett.*, 93:040503, Jul 2004.

⁹ Netanel H. Lindner and Terry Rudolph. Proposal for pulsed on-demand sources of photonic cluster state strings.

- Phys. Rev. Lett.*, 103:113602, Sep 2009.
- 10 Emil V. Denning, Jake Iles-Smith, Dara P. S. McCutcheon, and Jesper Mørk. Protocol for generating multiphoton entangled states from quantum dots in the presence of nuclear spin fluctuations. *Phys. Rev. A*, 96:062329, Dec 2017.
 - 11 Sean D. Barrett and Pieter Kok. Efficient high-fidelity quantum computation using matter qubits and linear optics. *Phys. Rev. A*, 71:060310, Jun 2005.
 - 12 Zhi-Rong Lin, Guo-Ping Guo, Tao Tu, Fei-Yun Zhu, and Guang-Can Guo. Generation of quantum-dot cluster states with a superconducting transmission line resonator. *Phys. Rev. Lett.*, 101:230501, Dec 2008.
 - 13 I. Schwartz, D. Cogan, E. R. Schmidgall, Y. Don, L. Gantz, O. Kenneth, N. H. Lindner, and D. Gershoni. Deterministic generation of a cluster state of entangled photons. *Science*, 2016.
 - 14 Sophia E Economou and Pratibha Dev. Spin-photon entanglement interfaces in silicon carbide defect centers. *Nanotechnology*, 27(50):504001, 2016.
 - 15 Giuseppe Vallone, Enrico Pomarico, Paolo Mataloni, Francesco De Martini, and Vincenzo Berardi. Realization and characterization of a two-photon four-qubit linear cluster state. *Phys. Rev. Lett.*, 98:180502, May 2007.
 - 16 XuBo Zou and W. Mathis. Generating a four-photon polarization-entangled cluster state. *Phys. Rev. A*, 71:032308, Mar 2005.
 - 17 Sophia E. Economou, Netanel Lindner, and Terry Rudolph. Optically generated 2-dimensional photonic cluster state from coupled quantum dots. *Phys. Rev. Lett.*, 105:093601, Aug 2010.
 - 18 M. Gimeno-Segovia, T. Rudolph, and S. E. Economou. Deterministic generation of large-scale entangled photonic cluster state from interacting solid state emitters. *ArXiv e-prints*, January 2018.
 - 19 Jake Iles-Smith, Dara P. S. McCutcheon, Ahsan Nazir, and Jesper Mørk. Phonon scattering inhibits simultaneous near-unity efficiency and indistinguishability in semiconductor single-photon sources. *Nature Photonics*, 11:521, Jul 2017. Article.
 - 20 Alexander V. Khaetskii, Daniel Loss, and Leonid Glazman. Electron spin decoherence in quantum dots due to interaction with nuclei. *Phys. Rev. Lett.*, 88:186802, Apr 2002.
 - 21 C. Testelin, F. Bernardot, B. Eble, and M. Chamorro. Hole-spin dephasing time associated with hyperfine interaction in quantum dots. *Phys. Rev. B*, 79:195440, May 2009.
 - 22 Jack Hansom, Carsten H. H. Schulte, Claire Le Gall, Clemens Matthiesen, Edmund Clarke, Maxime Hugues, Jacob M. Taylor, and Mete Atatüre. Environment-assisted quantum control of a solid-state spin via coherent dark states. *Nature Physics*, 10:725, Sep 2014.
 - 23 R. N. E. Malein, T. S. Santana, J. M. Zajac, A. C. Dada, E. M. Gauger, P. M. Petroff, J. Y. Lim, J. D. Song, and B. D. Gerardot. Screening nuclear field fluctuations in quantum dots for indistinguishable photon generation. *Phys. Rev. Lett.*, 116:257401, Jun 2016.
 - 24 I. A. Merkulov, Al. L. Efros, and M. Rosen. Electron spin relaxation by nuclei in semiconductor quantum dots. *Phys. Rev. B*, 65:205309, Apr 2002.
 - 25 P.F. Braun, X. Marie, L. Lombez, B. Urbaszek, T. Amand, P. Renucci, V. K. Kalevich, K. V. Kavokin, O. Krebs, P. Voisin, and Y. Masumoto. Direct observation of the electron spin relaxation induced by nuclei in quantum dots. *Phys. Rev. Lett.*, 94:116601, Mar 2005.
 - 26 EA Chekhovich, MN Makhonin, AI Tartakovskii, Amir Yacoby, H Bluhm, KC Nowack, and LMK Vandersypen. Nuclear spin effects in semiconductor quantum dots. *Nature materials*, 12(6):494, 2013.
 - 27 Bernhard Urbaszek, Xavier Marie, Thierry Amand, Olivier Krebs, Paul Voisin, Patrick Maletinsky, Alexander Högele, and Atac Imamoglu. Nuclear spin physics in quantum dots: An optical investigation. *Rev. Mod. Phys.*, 85:79–133, Jan 2013.
 - 28 Lorenza Viola, Emanuel Knill, and Seth Lloyd. Dynamical decoupling of open quantum systems. *Phys. Rev. Lett.*, 82:2417–2421, Mar 1999.
 - 29 W. M. Witzel and S. Das Sarma. Concatenated dynamical decoupling in a solid-state spin bath. *Phys. Rev. B*, 76:241303, Dec 2007.
 - 30 Wenxian Zhang, V. V. Dobrovitski, Lea F. Santos, Lorenza Viola, and B. N. Harmon. Dynamical control of electron spin coherence in a quantum dot: A theoretical study. *Phys. Rev. B*, 75:201302, May 2007.
 - 31 Götz S. Uhrig. Keeping a quantum bit alive by optimized π -pulse sequences. *Phys. Rev. Lett.*, 98:100504, Mar 2007.
 - 32 Götz S. Uhrig. Exact results on dynamical decoupling by pulses in quantum information processes. *New Journal of Physics*, 10(8):083024, 2008.
 - 33 Hendrik Bluhm, Sandra Foletti, Izhar Neder, Mark Rudner, Diana Mahalu, Vladimir Umansky, and Amir Yacoby. Dephasing time of gaas electron-spin qubits coupled to a nuclear bath exceeding 200 μ s. *Nature Physics*, 7:109, Dec 2010.
 - 34 R. Stockill, C. Le Gall, C. Matthiesen, L. Huthmacher, E. Clarke, M. Hugues, and M. Atatüre. Quantum dot spin coherence governed by a strained nuclear environment. *Nature Communications*, 7:12745, Sep 2016. Article.
 - 35 B. Eble, O. Krebs, A. Lemaître, K. Kowalik, A. Kudelski, P. Voisin, B. Urbaszek, X. Marie, and T. Amand. Dynamic nuclear polarization of a single charge-tunable InAs/GaAs quantum dot. *Phys. Rev. B*, 74:081306, Aug 2006.
 - 36 J. R. Petta, J. M. Taylor, A. C. Johnson, A. Yacoby, M. D. Lukin, C. M. Marcus, M. P. Hanson, and A. C. Gossard. Dynamic nuclear polarization with single electron spins. *Phys. Rev. Lett.*, 100:067601, Feb 2008.
 - 37 G. Éthier-Majcher, D. Gangloff, R. Stockill, E. Clarke, M. Hugues, C. Le Gall, and M. Atatüre. Improving a solid-state qubit through an engineered mesoscopic environment. *Phys. Rev. Lett.*, 119:130503, Sep 2017.
 - 38 Daniel Loss and David P. DiVincenzo. Quantum computation with quantum dots. *Phys. Rev. A*, 57:120–126, Jan 1998.
 - 39 Jan Fischer, W. A. Coish, D. V. Bulaev, and Daniel Loss. Spin decoherence of a heavy hole coupled to nuclear spins in a quantum dot. *Phys. Rev. B*, 78:155329, Oct 2008.
 - 40 E. A. Chekhovich, A. B. Krysa, M. S. Skolnick, and A. I. Tartakovskii. Direct measurement of the hole-nuclear spin interaction in single InP/GaInP quantum dots using photoluminescence spectroscopy. *Phys. Rev. Lett.*, 106:027402, Jan 2011.
 - 41 P. Fallahi, S. T. Yılmaz, and A. Imamoglu. Measurement of a heavy-hole hyperfine interaction in ingaas quantum dots using resonance fluorescence. *Phys. Rev. Lett.*, 105:257402, Dec 2010.
 - 42 C. Emary, Xiaodong Xu, D. G. Steel, S. Saikin, and L. J. Sham. Fast initialization of the spin state of an electron in a quantum dot in the voigt configuration. *Phys. Rev.*

- Lett.*, 98:047401, Jan 2007.
- ⁴³ G. Fernandez, T. Volz, R. Desbuquois, A. Badolato, and A. Imamoglu. Optically tunable spontaneous raman fluorescence from a single self-assembled InGaAs quantum dot. *Phys. Rev. Lett.*, 103:087406, Aug 2009.
- ⁴⁴ Z. Sun, A. Delteil, S. Faelt, and A. Imamoglu. Measurement of spin coherence using raman scattering. *Phys. Rev. B*, 93:241302, Jun 2016.
- ⁴⁵ Aymeric Delteil, Zhe Sun, Wei-bo Gao, Emre Togan, Stefan Faelt, and A. Imamoglu. Generation of heralded entanglement between distant hole spins. *Nature Physics*, 12:218, Dec 2015.
- ⁴⁶ R. Stockill, M. J. Stanley, L. Huthmacher, E. Clarke, M. Hugues, A. J. Miller, C. Matthiesen, C. Le Gall, and M. Atatüre. Phase-tuned entangled state generation between distant spin qubits. *Phys. Rev. Lett.*, 119:010503, Jul 2017.
- ⁴⁷ In practice, this assumption limits the size of the LCs that can be produced in this approach to less than ten.
- ⁴⁸ We assume η is the probability of obtaining a detector click if a photon was produced by the QD, i.e. it also includes any photon losses in the setup).
- ⁴⁹ The numerical calculations were performed using the Overhauser ensemble-averaged matrix operations defined in Appendix Sec C.
- ⁵⁰ M. Popp, F. Verstraete, M. A. Martín-Delgado, and J. I. Cirac. Localizable entanglement. *Phys. Rev. A*, 71:042306, Apr 2005.
- ⁵¹ Jonathan H. Prechtel, Andreas V. Kuhlmann, Julien Houel, Arne Ludwig, Sascha R. Valentin, Andreas D. Wieck, and Richard J. Warburton. Decoupling a hole spin qubit from the nuclear spins. *Nat Mater*, 15(9):981–986, Sep 2016. Article.
- ⁵² The anisotropy in the hole g-factor is, in general, not the same as the effective anisotropy in the g-tensor for the hole Overhauser shift due to hh lh mixing.
- ⁵³ the averages are performed independently due to the statistical independence of B_N^z and δT .
- ⁵⁴ Jake Iles-Smith, Dara P. S. McCutcheon, Jesper Mørk, and Ahsan Nazir. Limits to coherent scattering and photon coalescence from solid-state quantum emitters. *Phys. Rev. B*, 95:201305, May 2017.
- ⁵⁵ Admixture of conduction band states even in the absence of a lh contribution may result in a non-Ising type hyperfine Hamiltonian for the hh system⁵¹, however, this goes beyond the scope of this work.
- ⁵⁶ M. Zielinski, Y. Don, and D. Gershoni. Atomistic theory of dark excitons in self-assembled quantum dots of reduced symmetry. *Phys. Rev. B*, 91:085403, Feb 2015.
- ⁵⁷ M. A. Dupertuis, K. F. Karlsson, D. Y. Oberli, E. Pelucchi, A. Rudra, P. O. Holtz, and E. Kapon. Symmetries and the polarized optical spectra of exciton complexes in quantum dots. *Phys. Rev. Lett.*, 107:127403, Sep 2011.
- ⁵⁸ Y. Don, M. Zielinski, and D. Gershoni. The Optical Activity of the Dark Exciton. *ArXiv e-prints*, January 2016.
- ⁵⁹ E. A. Stinaff, M. Scheibner, A. S. Bracker, I. V. Ponomarev, V. L. Korenev, M. E. Ware, M. F. Doty, T. L. Reinecke, and D. Gammon. Optical signatures of coupled quantum dots. *Science*, 311(5761):636–639, 2006.
- ⁶⁰ H. J. Krenner, M. Sabathil, E. C. Clark, A. Kress, D. Schuh, M. Bichler, G. Abstreiter, and J. J. Finley. Direct observation of controlled coupling in an individual quantum dot molecule. *Phys. Rev. Lett.*, 94:057402, Feb 2005.
- ⁶¹ D. Kim, S. G. Carter, A. Greilich, A. S. Bracker, and Daniel Gammon. Ultrafast optical control of entanglement between two quantum-dot spins. *Nat Phys*, 7(3):223–229, Mar 2011.
- ⁶² R. Songmuang, S. Kiravittaya, and O. G. Schmidt. Formation of lateral quantum dot molecules around self-assembled nanoholes. *Applied Physics Letters*, 82(17):2892–2894, 2003.
- ⁶³ L. Wang, A. Rastelli, S. Kiravittaya, P. Atkinson, F. Ding, C. C. Bof Bufon, C. Hermannstaedter, M. Witzany, G. J. Beirne, P. Michler, and O. G. Schmidt. Towards deterministically controlled InGaAs/GaAs lateral quantum dot molecules. *New Journal of Physics*, 10(4):045010, 2008.
- ⁶⁴ Patrick M. Vora, Allan S. Bracker, Samuel G. Carter, Timothy M. Sweeney, Mijin Kim, Chul Soo Kim, Lily Yang, Peter G. Brereton, Sophia E. Economou, and Daniel Gammon. Spin-cavity interactions between a quantum dot molecule and a photonic crystal cavity. *Nature Communications*, 6:7665 EP, Jul 2015.
- ⁶⁵ Nakul Shaji, C. B. Simmons, Madhu Thalukulam, Levente J. Klein, Hua Qin, H. Luo, D. E. Savage, M. G. Lagally, A. J. Rimberg, R. Joynt, M. Friesen, R. H. Blick, S. N. Coppersmith, and M. A. Eriksson. Spin blockade and lifetime-enhanced transport in a few-electron si/sige double quantum dot. *Nature Physics*, 4:540, Jun 2008.
- ⁶⁶ A. Greilich, S. G. Carter, Danny Kim, A. S. Bracker, and D. Gammon. Optical control of one and two hole spins in interacting quantum dots. *Nat Photon*, 5(11):702–708, Nov 2011.
- ⁶⁷ K. M. Weiss, J. M. Elzerman, Y. L. Delley, J. Miguel-Sanchez, and A. Imamoglu. Coherent two-electron spin qubits in an optically active pair of coupled InGaAs quantum dots. *Phys. Rev. Lett.*, 109:107401, Sep 2012.
- ⁶⁸ J. M. Elzerman, K. M. Weiss, J. Miguel-Sanchez, and A. Imamoglu. Optical amplification using raman transitions between spin-singlet and spin-triplet states of a pair of coupled InGaAs quantum dots. *Phys. Rev. Lett.*, 107:017401, Jun 2011.
- ⁶⁹ A. N. Vamivakas, C.-Y. Lu, C. Matthiesen, Y. Zhao, S. Fält, A. Badolato, and M. Atatüre. Observation of spin-dependent quantum jumps via quantum dot resonance fluorescence. *Nature*, 467:297, Sep 2010.
- ⁷⁰ Danny Kim, Sophia E. Economou, Ștefan C. Bădescu, Michael Scheibner, Allan S. Bracker, Mark Bashkansky, Thomas L. Reinecke, and Daniel Gammon. Optical spin initialization and nondestructive measurement in a quantum dot molecule. *Phys. Rev. Lett.*, 101:236804, Dec 2008.
- ⁷¹ Projected gradient descent algorithms for quantum state tomography. *NPJ Quantum Information*, 3(1):44, 2017.
- ⁷² Daniel F. V. James, Paul G. Kwiat, William J. Munro, and Andrew G. White. Measurement of qubits. *Phys. Rev. A*, 64:052312, Oct 2001.
- ⁷³ M. Paris and J. Rehacek. *Quantum State Estimation*. Lecture Notes in Physics. Springer Berlin Heidelberg, 2004.